*photonics*

MDPI

*Article*

# Study on Side-Pumping and Electro-Optical Q-Switched Laser Performance of a Novel Near-Infrared Laser Crystal Nd:GYSAG

**Jianling Gu [1], Haiyue Wang [2,*], Lei Huang [3,4,5,*], Qingli Zhang [4,5] and Guihua Sun [4,5]**

1 Technology Innovation Management Department, Hebei Expressway Group Co., Ltd., Shijiazhuang 050081, China; gujianling1983@163.com
2 Business Development Department, Hebei Expressway Group Co., Ltd., Jingqin Branch, Qinhuangdao 066000, China
3 School of Environmental Science and Optoelectronic Technology, University of Science and Technology of China, Hefei 230026, China
4 Anhui Provincial Key Laboratory of Photonic Devices and Materials, Anhui Institute of Optics and Fine Mechanics, Hefei Institutes of Physical Science, Chinese Academy of Sciences, Hefei 230031, China; zql@aiofm.ac.cn (Q.Z.); ghsun@aiofm.ac.cn (G.S.)
5 Advanced Laser Technology Laboratory of Anhui Province, Hefei 230037, China
* Correspondence: m18630331117@163.com (H.W.); hlogle@mail.ustc.edu.cn (L.H.)

**Abstract**

The Nd:GYSAG crystal enables multi-wavelength near-infrared laser output, with adjustable wavelengths tailored for specific application requirements, making it highly valuable for space-borne water vapor detection. This study reports, for the first time, the side-pumping characteristics and electro-optical Q-switching performance of this crystal. Using Ø3 × 73 mm and Ø4 × 73 mm crystal rods doped with 1.21 at.% Nd:GYSAG (chemical formula $Nd_{0.033}Gd_{0.93}Y_{1.79}Sc_{0.70}Al_{4.54}O_{11.99}$), 1060.4 nm laser output was achieved under 808 nm laser diode (LD) side-pumping at a repetition rate of 100 Hz and a pump pulse width of 250 μs. The experimental results show that the Ø4 × 73 mm rod had a higher laser threshold but exhibited significantly superior slope efficiency and maximum output power compared to the Ø3 × 73 mm rod. Using a flat–flat resonator, optimal laser performance was obtained with an output coupler transmission of 35%, yielding a slope efficiency of 37.2%. A maximum output energy of 179.4 mJ was achieved at a pump energy of 646 mJ. Thermal lensing effects were compensated using a flat–convex cavity, leading to improved laser performance and beam quality. Electro-optical Q-switching experiments were conducted using a KD*P crystal. A comparison between voltage-applied and voltage-removed Q-switching techniques revealed superior performance for the voltage-applied method. High-performance laser output was realized, achieving a maximum pulse energy of 59.6 mJ, a pulse width of 14.93 ns, and a peak power of 3.99 MW. This study provides an important foundation for the development of near-infrared laser devices based on Nd:GYSAG.

**Keywords:** Nd:GYSAG; side-pumping; electro-optical Q-switching; near-infrared

Check for updates

Received: 24 January 2026
Revised: 17 February 2026
Accepted: 22 February 2026
Published: 16 March 2026

**Copyright:** © 2026 by the authors. Licensee MDPI, Basel, Switzerland. This article is an open access article distributed under the terms and conditions of the Creative Commons Attribution (CC BY) license.

## 1. Introduction

The neodymium-doped gadolinium scandium aluminum garnet (Nd:GSAG) laser gain medium can be directly pumped by laser diodes (LD) to generate a 942 nm laser wavelength corresponding to water vapor absorption. Through wavelength tuning, it can achieve strong, medium, and weak water vapor absorption intensities, making it suitable for differential absorption lidar (DIAL) in water vapor detection [1–10]. Nd:GYSAG (chemical formula: $(Nd_xGd_yY_{1-x-y})_3Sc_zAl_{5-z}O_{12}$) is a novel laser crystal derived from Nd:GSAG,

Nd:YSAG, and Nd:YAG crystals. For these three crystals, the primary emission peaks corresponding to the $^4F_{3/2} \rightarrow {}^4I_{9/2}$ transition of $Nd^{3+}$ ions are located at 942 nm, 942 nm, and 946 nm, respectively. In contrast, the main emission peak of Nd:GYSAG lies between 942 nm and 946 nm. By adjusting its composition, it is expected to precisely match the strong water vapor absorption peaks at 943.082 nm or 944.368 nm [11–19]. Furthermore, increasing the degree of structural disorder in the crystal can effectively broaden the full width at half maximum (FWHM) of the emission spectrum, enhancing wavelength tuning capability. This makes it more advantageous for water vapor detection using DIAL. When pumped by 808 nm laser diodes (LD), Nd:GSAG, Nd:YSAG, and Nd:YAG crystals can generate laser outputs at 1060 nm, 1059 nm, and 1064 nm, respectively. The primary emission peak of Nd:GYSAG falls between 1059 nm and 1064 nm. Through compositional tuning, it is possible to adjust the fundamental laser wavelength and achieve dual-wavelength laser output, which can then be used for terahertz wave generation via difference-frequency generation (DFG) [20].

In 2024, Conghui Huang et al. first reported the spectroscopic properties and dual-wavelength laser performance of a novel Nd:$Gd_{1.8}Y_{1.2}Sc_2Al_4O_{12}$ (Nd:GYSAG) crystal [21]. The crystal achieved 5.02 W of continuous-wave (CW) laser output at 1061.2 nm and 1063.2 nm under an absorbed pump power of 9.45 W, with a slope efficiency of 59.4% and an optical-to-optical efficiency of 53.1%. Using Cr:YAG as a saturable absorber (SA), stable passively Q-switched (PQS) laser operation was realized, yielding a maximum average output power of 0.756 W, a slope efficiency of 34.4%, and pulse characteristics of 14.0 ns pulse width, 128.1 μJ pulse energy, and 9.15 kW peak power. These results demonstrate that Nd:GYSAG is an excellent laser medium for high-efficiency dual-wavelength laser generation, with potential applications in terahertz (THz) laser production. In 2025, Wenfang Lin et al. further investigated the spectroscopic properties and tunable laser performance of Nd:GYSAG (Nd:$Gd_{1.8}Y_{1.2}Sc_2Al_4O_{12}$) [22]. Leveraging its spectral characteristics, discrete wavelength tuning (1048–1120 nm) was achieved in a three-mirror folded cavity using a birefringent filter. The incorporation of $Y^{3+}$ ions introduced greater structural disorder, leading to inhomogeneous spectral broadening and similar emission cross-sections at different Stark levels. This property enhanced the multi-wavelength laser efficiency. Compared to Nd:GSAG, Nd:GYSAG exhibited higher output power, improved efficiency, and a broader tunable range.

High-energy laser output can be expected via LD side-pumping, and pulsed laser with high precision and low energy jitter can be achieved through electro-optical (EO) Q-switching. These advantages have been demonstrated in Nd:GSAG crystals, whereas no related research has been reported on Nd:GYSAG crystals [1]. In this work, we employ a newly doped Nd:GYSAG crystal rod (chemical formula: $Nd_{0.033}Gd_{0.93}Y_{1.79}Sc_{0.70}Al_{4.54}O_{11.99}$) for laser experiments under 808 nm pulsed LD side-pumping. We compare the laser performance of Φ3 × 73 mm and Φ4 × 73 mm samples with different output coupler transmittances. By optimizing the plano-convex cavity, we improve laser efficiency and beam quality. Additionally, using KD*P as an EO Q-switch, we achieve a stable Q-switched laser output.

## 2. Experiment

### *2.1. Crystal Rod*

The laser experiments employed a 1.21 at.% Nd:GYSAG gain medium grown by the Czochralski method. The crystal was grown using high-purity starting reagents of $Gd_2O_3$, $Y_2O_3$, $Sc_2O_3$, $Al_2O_3$, and $Nd_2O_3$ with a purity of 99.999% (5N). The growth process was performed under a nitrogen ($N_2$) atmosphere. The chemical composition of the as-grown crystal was determined to be $Nd_{0.033}Gd_{0.93}Y_{1.79}Sc_{0.70}Al_{4.54}O_{11.99}$. The crystal was processed

into cylindrical rods along the [111] crystallographic direction (as shown in Figure 1), with dimensions of 73 mm in length and diameters of 3 mm and 4 mm. Both end faces were coated with anti-reflection (AR) coatings optimized for 942 nm and 1060 nm wavelengths.

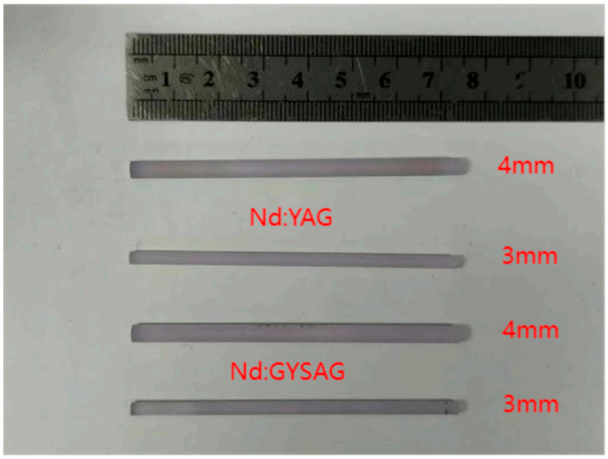



**Figure 1.** Nd:GYSAG crystal rod. (Φ3 × 73 mm and Φ4 × 73 mm).

### *2.2. Side-Pumping Experimental Setup*

The experimental setup employed an 808 nm semiconductor side-pumping laser module (Model SLD-3 × 7-4, Beijing Leike Optoelectronic Technology Co., Ltd., Beijing, China), as shown in Figure 2. The repetition rate was fixed at 100 Hz since the single-pulse energy remained nearly constant with frequency variation. The pulse width was set to 250 μs to maximize the output energy, yielding a maximum pump energy of 646 mJ. Temperature control was achieved through an internal water cooling system maintained at 293.15 ± 1 K. The laser resonator consisted of a high-reflectivity (HR) mirror (1060–1064 nm) and a partial-transmission output coupler (1060–1064 nm), with a cavity length of 90 mm. Laser output power was measured using an Ophir 30A-BB-18 power meter (Ophir Optronics Solutions, North Logan, UT, USA), while spectral characteristics were analyzed with an Avantes multichannel spectrometer (Avantes BV, Apeldoorn, The Netherlands). Beam quality was evaluated using a Spiricon M2-200S-FW beam profiler system (Ophir-Spiricon LLC, North Logan, UT, USA), which provided $M^2$ factor determination through integrated software algorithms.

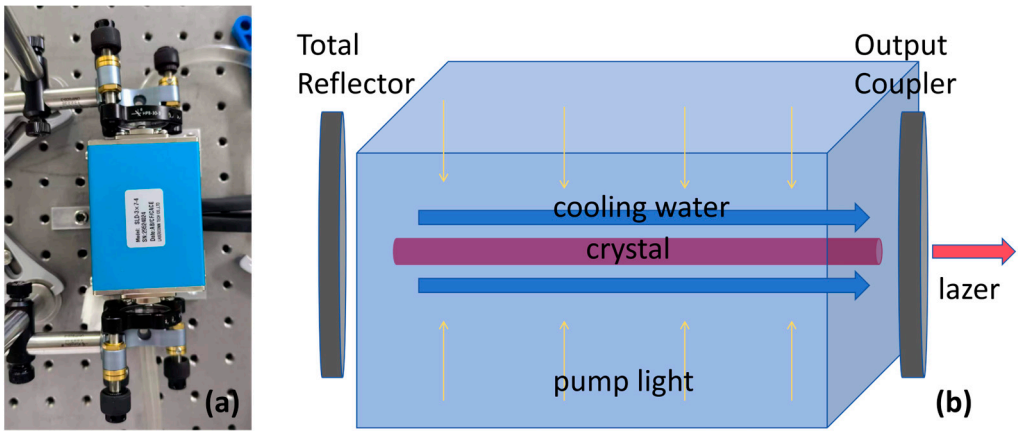



**Figure 2.** Scheme of Semiconductor Side Pump Module and Experimental Device (**a**) Photograph; (**b**) Schematic Scheme.

### *2.3. Electro-Optical Q-Switching Experimental Setup*

The experimental setup for electro-optic Q-switching is illustrated in Figure 3. The laser gain medium was a Φ4 mm sample, and the optical resonator employed a plano-plano cavity configuration with an output coupler exhibiting 35% transmittance at 1064 nm. The Q-switching system incorporated a KD*P crystal operated in both voltage-applied and voltage-removed modes, driven by LH-J2K (voltage-applied) and LH-T2K (voltage-removed) Q-switch modules (Shenzhen Aikex Technology Co., Ltd., Shenzhen, China, 2 kHz repetition rate). A polarizing beam splitter (PBS) served as the polarizer. To ensure operational safety and prevent optical damage, the Q-switch crystal, quarter-wave plate, and polarizer were all positioned at the high-reflector end of the cavity. The resonator length was minimized to 160 mm using customized components to enhance system stability and efficiency. Theoretical calculations confirmed that the thermal focal length of the crystal significantly exceeded the distance between the crystal center and the high-reflector, ensuring stable cavity operation throughout experiments. By positioning the output coupler in close proximity to the crystal, this design effectively suppressed higher-order modes while improving beam quality and energy conversion efficiency. Temporal pulse characteristics were measured using a silicon photodetector (THORLABS-DET10A/M, Thorlabs, Inc., Newton, NJ, USA).

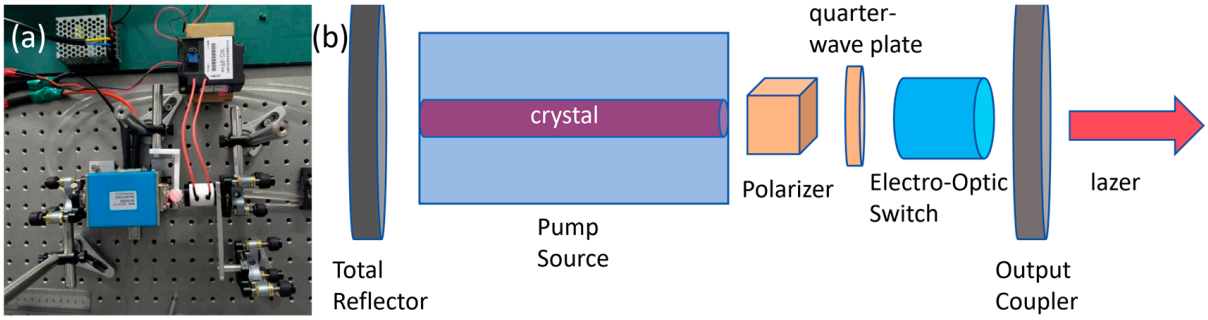



**Figure 3.** Scheme of Electro-optic Q-switching Experimental Device. (**a**) Photograph; (**b**) Schematic Scheme.

## 3. Results and Discussion

### *3.1. Laser Performance*

At a laser output energy of 20 mJ, spectral characterization with a spectrometer resolution of 0.1 nm revealed single-wavelength operation at 1060.4 nm, with a full width at half maximum (FWHM) bandwidth of 0.48 nm, as shown in Figure 4.

Figure 5 presents the laser output energy versus pump energy for the Φ4 × 73 mm crystal rod. Optimal performance was achieved using an output coupler with 35% transmittance, yielding a maximum output energy of 179.4 mJ with a corresponding optical-to-optical conversion efficiency of 27.0%, slope efficiency of 37.2%, and a lasing threshold of 176.5 mJ. Notably, the pump wavelength exhibited a redshift from 806 nm to 809 nm with increasing pump power, progressively approaching the crystal's absorption peak at 808.6 nm, which contributed to enhanced slope efficiency.

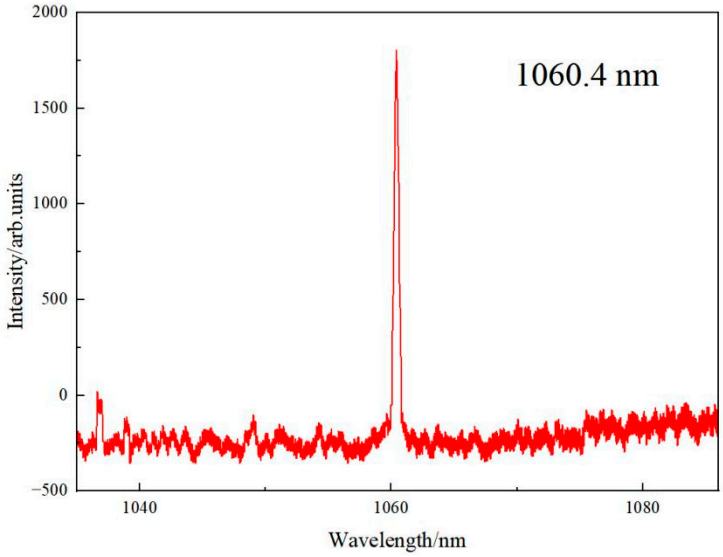



**Figure 4.** The wavelength of the laser.

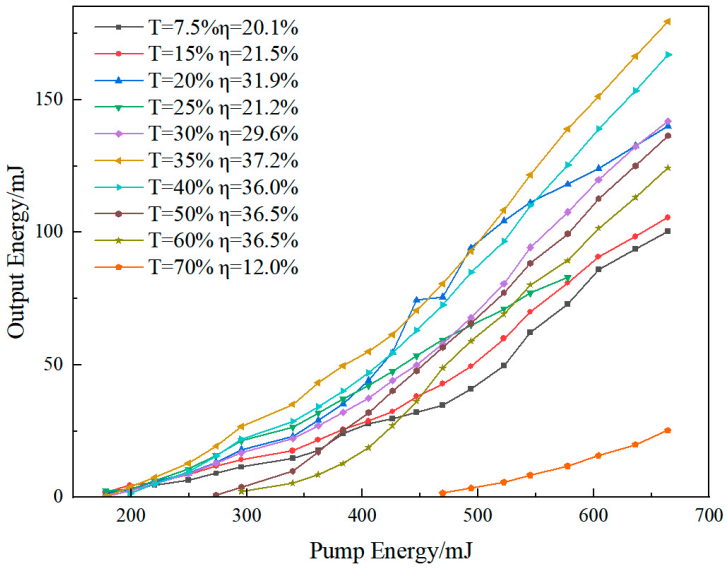



**Figure 5.** The variation in output energy of Nd: GYSAG (Φ4 × 73 mm) laser with pump energy under different transmittance.

Figure 6 displays the experimental results for the Φ3 × 73 mm crystal rod. Compared to the Φ4 × 73 mm rod, the smaller-diameter rod demonstrated a significantly lower lasing threshold (116.7 mJ with 40% output coupler transmittance) but exhibited reduced overall performance with maximum output energy of 107.8 mJ, optical-to-optical conversion efficiency of 16.2%, and slope efficiency of 19.5%. The thermal lensing effect was more pronounced in the Φ3 × 73 mm Nd:GYSAG rod compared to the Φ4 × 73 mm counterpart. Specifically, as the pump power increased, the thermal focal length of the Φ3 × 73 mm rod exhibited a continuous and significant reduction. This intense thermal lensing effect not only distorted the laser beam wavefront but also exacerbated the mismatch between the fundamental cavity mode size and the crystal cross-sectional area. Although the pump wavelength redshift (a beneficial factor for reducing quantum defect and mitigating thermal load) was observed, its positive impact was overwhelmed by the severe thermal lensing-induced diffraction loss and mode distortion. Consequently, the slope efficiency of the Φ3 × 73 mm rod showed a progressive decline with increasing pump power.

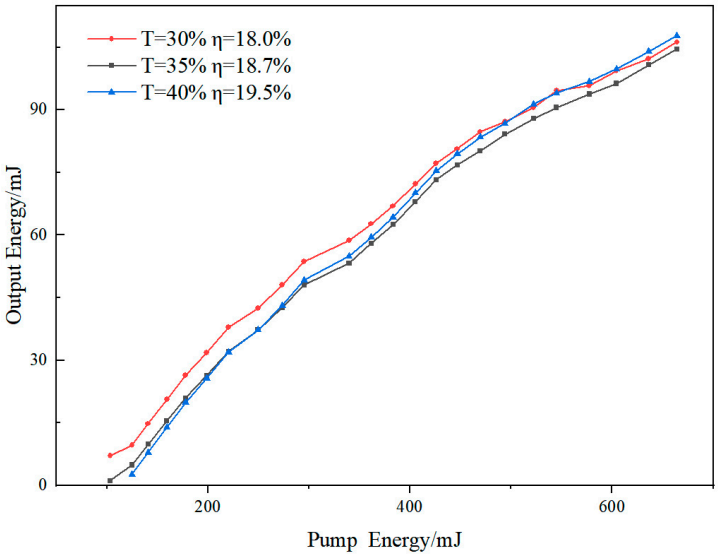



**Figure 6.** The variation in output energy of Nd: GYSAG (Φ3 × 73 mm) laser with pump energy under different transmittance.

### *3.2. Plano-Convex Resonators*

To compensate for thermal lensing effects, a plano-convex output coupler with 1000 mm curvature radius and 40% transmittance at 1064 nm was employed. Figure 7 compares the output characteristics between plano-plano and plano-convex cavities. In the Φ4 × 73 mm crystal, the plano-convex cavity achieved a maximum output power of 175.2 mJ with 26.4% optical-to-optical efficiency and 40.1% slope efficiency, representing a 4.1% improvement over the plano-plano configuration. The lasing threshold was 209.7 mJ. For the Φ3 × 73 mm crystal, the plano-convex cavity demonstrated 119.2 mJ maximum output power with 17.9% optical-to-optical efficiency and 22.9% slope efficiency (3.4% improvement), with a threshold of 127.9 mJ.

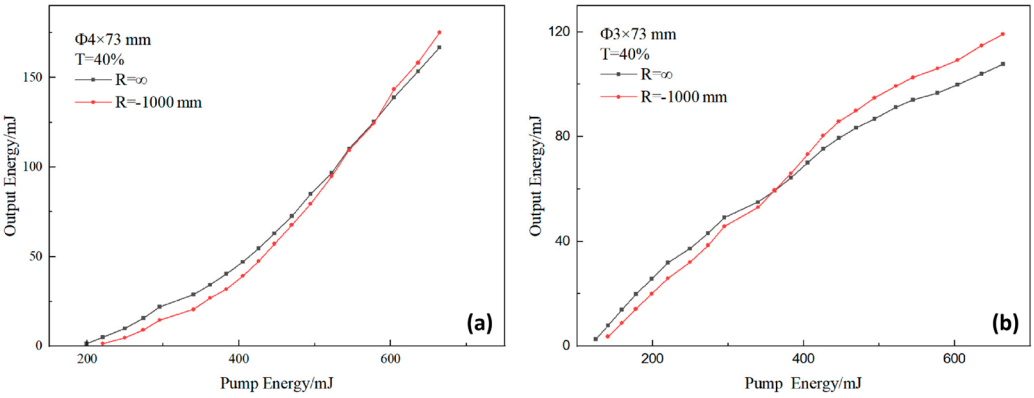



**Figure 7.** Output energy of flat and convex cavity lasers. (**a**) Φ4 × 73 mm; (**b**) Φ3 × 73 mm.

The thermal lensing effect was more pronounced in the smaller Φ3 × 73 mm crystal, where the plano-convex cavity provided greater relative performance enhancement compared to the Φ4 × 73 mm crystal. At low pump powers, the plano-convex cavity showed reduced output due to the long thermal focal length, but outperformed the plano-plano cavity at higher pump powers as the thermal focal length decreased. This demonstrates the effectiveness of curvature compensation, particularly for crystals exhibiting stronger thermal lensing effects.

We conducted systematic measurements of the laser beam diameter and beam quality factor $M^2$ for the Φ4 × 73 mm crystal in both plano-plano and plano-convex cavity config-

urations. Figure 8 presents the variation in $M^2$ with pump power, while Figure 9 shows the beam diameter propagation characteristics at the maximum pump energy of 646 mJ.

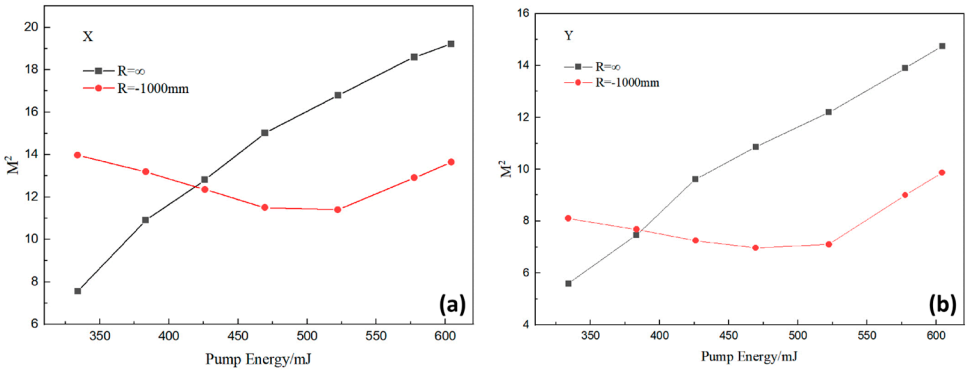



**Figure 8.** The beam quality of flat and convex cavities. (**a**) X direction; (**b**) Y direction.

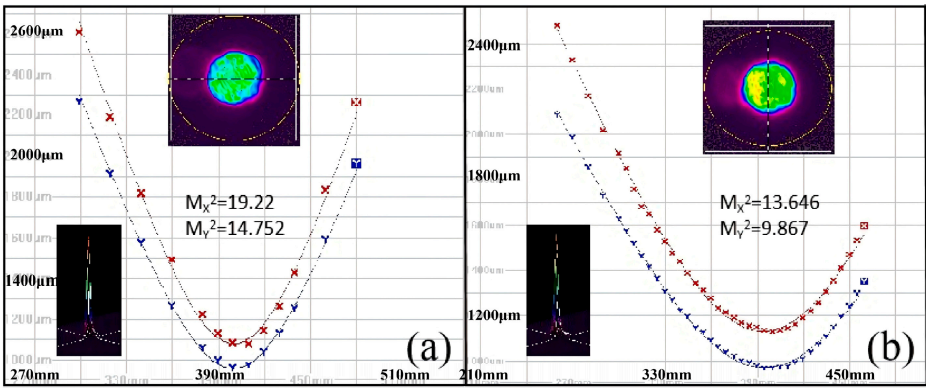



**Figure 9.** The variation in laser spot diameter with propagation distance in the LD side-pumped Nd:GYSAG crystal. (**a**) Flat cavity; (**b**) flat convex cavity.

In the plano-plano cavity, the beam quality progressively deteriorated with increasing pump power, as evidenced by the rising $M^2$ values. At the maximum pump energy of 646 mJ, the beam quality factors reached $M_x^2$ = 19.22 and $M_y^2$ = 14.75. The plano-convex cavity initially exhibited poorer beam quality at low pump powers, but demonstrated significant improvement as the pump power increased and the thermal lens compensation became effective. However, when the pump power exceeded certain levels, the thermal lensing effect surpassed the compensation capability of the plano-convex design, leading to renewed degradation in beam quality. At 646 mJ pump energy, the plano-convex cavity achieved superior beam quality factors of $M_x^2$ = 13.65 and $M_y^2$ = 9.87, representing substantial improvement over the plano-plano configuration under high pump power conditions. These results clearly demonstrate that the plano-convex cavity design effectively mitigates thermal lensing effects and maintains better beam quality during high-power operation, though its compensation capability has limitations at extremely high pump powers. The beam propagation measurements confirm that proper cavity design can significantly enhance the spatial characteristics of laser output in side-pumped systems.

### *3.3. Electrical Light Q-Switching*

The Q-switched laser output characteristics are presented in Figure 10. Figure 10a shows the laser output energy versus pump energy, while Figure 10b displays the pulse width variation with pump energy. The temporal profiles include: free-running operation with 217.5 μs pulse width (Figure 10c), maximum output power operation with 14.93 ns

pulse width under voltage-applied Q-switching (Figure 10d), and the Q-switched pulse train at 100 Hz repetition rate (Figure 10e).

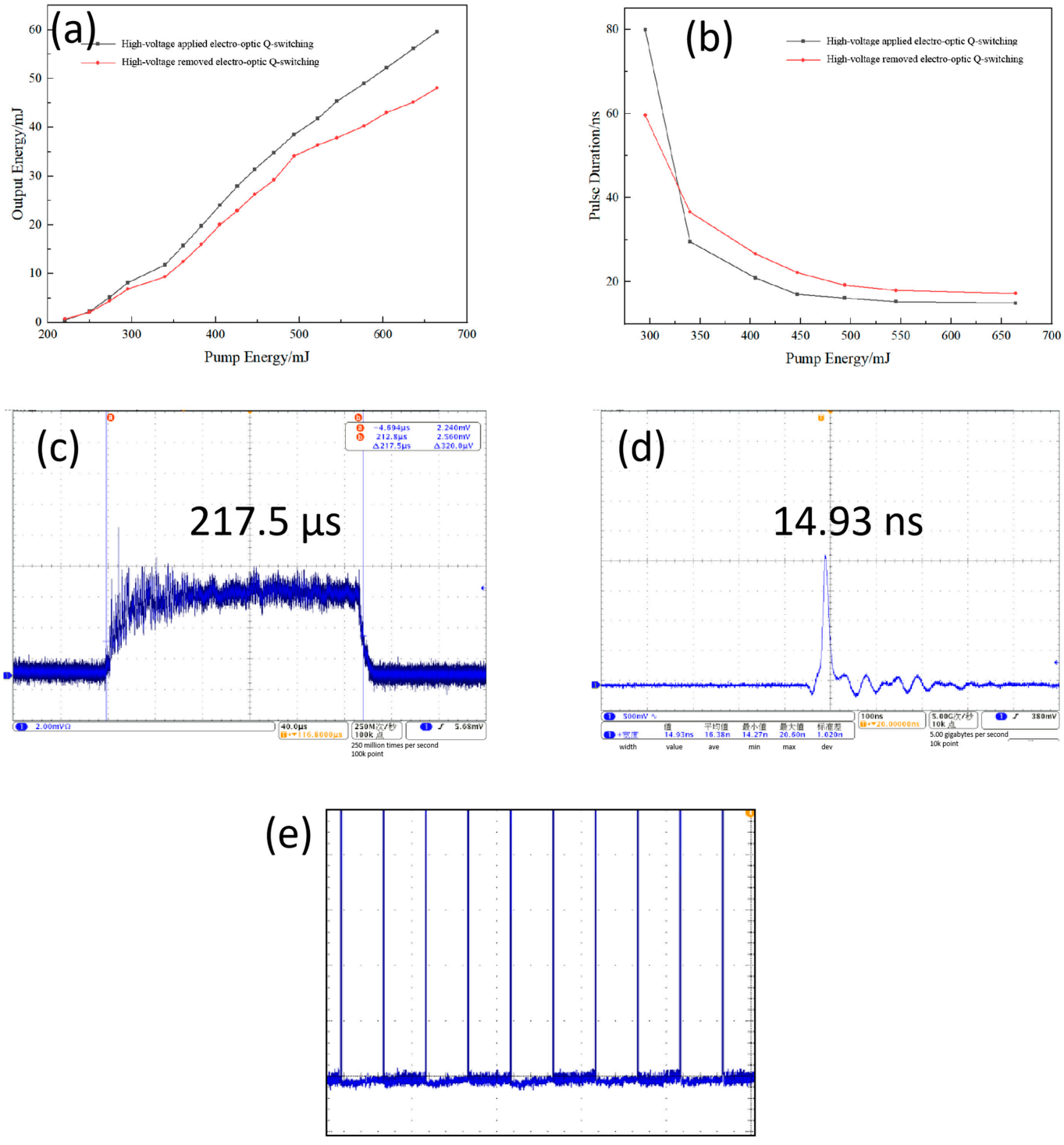



**Figure 10.** Q-switched laser output characteristics. (**a**) Variation in laser output energy with pump energy; (**b**) pulse width varies with pump energy; (**c**) pulse waveform of free-running laser; (**d**) pulse waveform after Q adjustment; and (**e**) pulse sequence.

Comparative analysis revealed superior performance of the voltage-applied Q-switching mode over the voltage-removed mode in both output energy and pulse width. The performance discrepancy stems from the intrinsic operational characteristics of the two modes: (1) The voltage-removed mode requires continuous application of high voltage, which in-

duces thermal effects and leakage current in the electro-optic crystal. These issues degrade the switching-off efficiency and cause weak oscillation, leading to non-radiative loss of upper-level population. (2) The voltage-removed mode is highly sensitive to the accuracy of the 1/4λ voltage and the polarization matching degree of the resonator, resulting in inferior switching-off performance under practical non-ideal conditions. In contrast, the voltage-applied mode operates at a static zero-voltage state in the off-phase, which minimizes the thermal load on the electro-optic crystal and ensures long-term operational stability. This mode achieves cleaner switching-off, effectively suppressing weak oscillation and population loss, ultimately yielding narrower pulse widths and higher single-pulse energy. The voltage-applied Q-switching configuration achieved threshold energy of 213.6 mJ, slope efficiency of 14.2%, maximum output energy of 59.6 mJ, and peak power of 3.99 MW. For comparison, previous studies based on passive Q-switching and end-pumping configurations have reported a maximum average output power of 0.756 W, a slope efficiency of 34.4%, and pulse characteristics including 14.0 ns pulse width, 128.1 μJ pulse energy, and 9.15 kW peak power [22]. The differences in laser performance between this work and previous reports are mainly attributed to the distinct pumping schemes (side-pumping vs. end-pumping) and Q-switching technologies (EO Q-switching vs. passive Q-switching).

## 4. Conclusions

This study presents a comprehensive investigation of the side-pumped and electro-optically Q-switched laser performance of Nd:GYSAG crystals. Systematic experiments were conducted using 1.21 at.% Nd:GYSAG crystal rods with different dimensions (Φ3 × 73 mm and Φ4 × 73 mm) under various output coupler transmittances. The optimal laser performance was achieved with the Φ4 × 73 mm rod and 35% output coupler transmittance, yielding 179.4 mJ maximum output energy at 100 Hz repetition rate with 37.2% slope efficiency. Beam quality was significantly improved through the implementation of a plano-convex cavity design. Furthermore, comparative analysis of voltage-applied and voltage-removed electro-optic Q-switching techniques demonstrated superior performance of the voltage-applied approach. The optimized Q-switched operation produced laser pulses with 59.6 mJ energy, 14.93 ns pulse width, and 3.99 MW peak power at 100 Hz repetition rate. These results establish Nd:GYSAG as an efficient gain medium for high-energy, high-peak-power laser systems, while providing practical insights for optimizing both continuous-wave and Q-switched operations through appropriate resonator design and Q-switch control methods.

**Author Contributions:** Conceptualization, Q.Z. and G.S.; methodology, Q.Z.; software, Q.Z.; validation, H.W., Q.Z. and G.S.; formal analysis, G.S.; investigation, J.G.; resources, J.G.; data curation, L.H.; writing—original draft preparation, L.H.; writing—review and editing, L.H.; visualization, J.G.; supervision, H.W.; project administration, H.W.; funding acquisition, H.W. All authors have read and agreed to the published version of the manuscript.

**Funding:** This research was funded by the S&T Program of Hebei, grant number 23280802Z.

**Data Availability Statement:** The original contributions presented in this study are included in the article. Further inquiries can be directed to the corresponding authors.

**Conflicts of Interest:** Author Haiyue Wang is employed by the Business Development Department, Hebei Expressway Group Co., Ltd. Author Haiyue Wang declares no financial or non-financial conflicts of interest. The remaining authors certify that no commercial, personal, or professional relationships influenced the research design, data interpretation, or conclusions of this study. All funding sources are disclosed in the Funding section.

## Abbreviations

The following abbreviation is used in this manuscript:

LD Linear dichroism

## References


1. Chu, C.; Fu, X.; Li, Y. Diode-pumped continuous-wave Nd:GSAG lasers operating at 1.4 μm. *Opt. Laser Technol.* **2025**, *181*, 111846. [CrossRef]
2. Huang, L.; Zhang, Q.; Dou, R.; Luo, J.; Zhang, J.; Liu, Y.; Zhang, R.; Shao, J.; Sun, G.; Liu, W. Improvement of surface morphology and laser performance of garnet laser crystals by 193 nm ArF excimer laser processing. *Opt. Laser Technol.* **2024**, *179*, 111138. [CrossRef]
3. Huang, C.; Lin, W.; Zhang, S.; Fang, Q.; Tao, S.; Xu, M.; Li, S.; Zhao, C.; Hang, Y. Efficient continuous-wave and passively Q-switched Nd:GSAG laser operating at 1.3 μm. *Opt. Laser Technol.* **2024**, *177*, 111061. [CrossRef]
4. Dou, R.; Huang, L.; Liu, Y.; Gao, J.; Wang, X.; Zhang, D.; Luo, J.; Liu, W.; Jiang, H.; Zhang, Q. Crystal growth and laser properties of gradual concentration Nd-doped yttrium aluminum garnet serial crystals. *Opt. Laser Technol.* **2024**, *170*, 110227. [CrossRef]
5. Huang, C.; Lin, W.; Fang, Q.; Xu, M.; Zhang, S.; Tao, S.; Li, S.; Zhao, C.; Hang, Y. Spectroscopic properties and discrete multi-wavelength tuning lasers of Nd:GSAG. *Opt. Laser Technol.* **2023**, *164*, 109484. [CrossRef]
6. Wang, B.; Liu, W.; Ren, H.; Zhang, C.; Liu, H.; Zou, Y.; Ding, S. Morphologies and Formation Mechanisms of the Defects in Gadolinium-Scandium-Aluminum Garnet Single Crystal. *J. Synth. Cryst.* **2022**, *51*, 1851–1857.
7. Xu, J. Growth and Optical Performance of New-Type Laser Crystal Nd:GSAG and Cr,Nd:GSAG. Master's Thesis, University of Science and Technologyof China, Hefei, China, 2017.
8. Xu, J.; Zhang, Q.; Peng, F.; Wang, X.; Dou, R.; Luo, J.; Sun, G.; Ding, S.; Sun, D. Growth, Spectral Properties and LD Pumped Laser Performances of Cr,Nd:GSAG Crystal. *J. Synth. Cryst.* **2017**, *46*, 1653–1659.
9. Xiao, J.; Zhang, Q.; Zhou, W.; Tan, X.; Liu, W.; Yin, S.; Jiang, H.; Xia, S.; Guo, C. Crystal field energy-levels of $Nd^{3+}$:$Gd_3Sc_2Al_3O_{12}$ and fitting. *Acta Phys. Sin.* **2010**, *59*, 7306–7313.
10. AbdulRazzaq, M.J.; Mohammed, A.Z.; Abass, A.K.; Shibib, K.S. A new approach to evaluate temperature distribution and stress fracture within solid state lasers. *Opt. Quantum Electron.* **2019**, *51*, 294. [CrossRef]
11. Lu, W.; Zhang, Q.; Luo, J.; Ding, S.; Dou, R.; Peng, F.; Zhang, H.; Wang, X.; Sun, G.; Sun, D. Spectral and laser properties of Nd:YSAG single crystal. *Acta Phys. Sin.* **2017**, *66*, 146–151.
12. Wen, Y.; Li, T.; He, Q.; Zhang, H.; Wang, C.; Wu, C.; Jin, G. Laser-diode dual-end-pumped electro-optic Q-switched slab Tm:YAP laser. *Infrared Phys. Technol.* **2020**, *105*, 103215. [CrossRef]
13. Solomon, S.; Rosenlof, K.H.; Portmann, R.W.; Daniel, J.S.; Davis, S.M.; Sanford, T.J.; Plattner, G.-K. Contributions of Stratospheric Water Vapor to Decadal Changes in the Rate of Global Warming. *Science* **2010**, *327*, 1219–1223. [CrossRef] [PubMed]
14. Vogelmann, H.; Trickl, T. Wide-range sounding of free-tropospheric water vapor with a differential-absorption lidar (DIAL) at a high-altitude station. *Appl. Opt.* **2008**, *47*, 2116–2132. [CrossRef] [PubMed]
15. Wang, J.; Wang, K.; Pielke, R.A.; Lin, J.C.; Matsui, T. Towards a robust test on North America warming trend and precipitable water content increase. *Geophys. Res. Lett.* **2008**, *35*, L18804. [CrossRef]
16. Willett, K.M.; Jones, P.D.; Gillett, N.P.; Thorne, P.W. Recent Changes in Surface Humidity: Development of the HadCRUH Dataset. *J. Clim.* **2008**, *21*, 5364–5383. [CrossRef]
17. Willett, K.M.; Gillett, N.P.; Jones, P.D.; Thorne, P.W. Attribution of observed surface humidity changes to human influence. *Nature* **2007**, *449*, 710–712. [CrossRef]
18. Koechner, W. *Solid-State Laser Engineering*, 6th ed.; Springer: New York, NY, USA, 2006.
19. Held, I.M.; Soden, B.J. Water Vapor Feedback and Global Warming. *Annu. Rev. Energy Environ.* **2000**, *25*, 441–475. [CrossRef]
20. Wei, M.-E.; Cheng, T.-Q.; Dou, R.-Q.; Zhang, Q.-L.; Jiang, H.-H. High-peak-power electro-optically Q-switched laser with a gradient-doped Nd:YAG crystal. *Opt. Lett.* **2021**, *46*, 5016–5018. [PubMed]
21. Huang, C.; Lin, W.; Fang, Q.; Xu, M.; Zhang, S.; Tao, S.; Li, S.; Zhao, C.; Hang, Y. Spectroscopy and efficient dual-wavelength laser performances of a Nd:GYSAG crystal. *Opt. Lett.* **2024**, *49*, 2994–2997. [CrossRef] [PubMed]
22. Lin, W.; Huang, C.; Li, S.; Tao, S.; Chen, G.; Xu, M.; Zhao, C.; Fang, Q.; Ye, X.; Hang, Y. Efficient discrete tuning lasers of Nd:GYSAG crystal in 1 μm wavelength region. *Infrared Phys. Technol.* **2025**, *145*, 105682. [CrossRef]


**Disclaimer/Publisher's Note:** The statements, opinions and data contained in all publications are solely those of the individual author(s) and contributor(s) and not of MDPI and/or the editor(s). MDPI and/or the editor(s) disclaim responsibility for any injury to people or property resulting from any ideas, methods, instructions or products referred to in the content.